Carbon-13 Solid-State NMR Studies on Synthetic Model Compounds of [4Fe−4S] Clusters in the 2+ State

Marielle Crozet,[†,‡] Marc Chaussade,[†,§] Michel Bardet,[∥] Lyndon Emsley,[⊥] Bernard Lamotte,[*,†] and Jean-Marie Mouesca[†]

Service de Chimie Inorganique et Biologique, UMR 5046, Département de Recherche Fondamentale sur la Matière Condensée, CEA-Grenoble, 17 rue des Martyrs, 38054 Grenoble Cedex 9, France, Laboratoire des Lésions des Acides Nucléiques, Service de Chimie Inorganique et Biologique, Département de Recherche Fondamentale sur la Matière Condensée, CEA-Grenoble, 17 rue des Martyrs, 38054 Grenoble Cedex 9, France, and Laboratoire de Stéréochimie et des Interactions Moléculaires, UMR 5532 CNRS/ENS, Ecole Normale Supérieure de Lyon, 46 Allée d'Italie, 69364 Lyon Cedex 07, France

Received: June 2, 2000

Carbon-13 solid-state NMR is used to determine, via the temperature dependence of paramagnetic shifts, the spin ladder of magnetic levels and the related spin exchange parameters in $[4Fe-4S]^{2+}$ clusters. This study has been carried out between 180 and 330 K in three model compounds of the active sites of 4Fe−4S proteins: $[(C_2D_5)_4N]_2[Fe_4S_4(S^{13}CD_2C_6D_5)_4]$, $[(C_2H_5)_4N]_2[Fe_4S_4(SC(CH_3)_3)_4]$, and $[(C_2H_5)_4N]_2[Fe_4Se_4(SC(CH_3)_3)_4]$. The temperature dependencies of both the isotropic and anisotropic parts of the ^{13}C paramagnetic shift tensors have been measured and analyzed. Antiferromagnetic exchange coupling constants among iron atoms of $J \approx 430$, 380, and 370 cm^{-1} have been deduced from fits of their temperature dependencies. Additional contributions of the double-exchange term B favoring electronic delocalization and of a ΔJ term associated with the compression of the cubane geometry are also discussed. We also show that connections between these measurements and those of magnetic susceptibility are especially close in the case of the $[4Fe-4S]^{2+}$ redox state.

I. Introduction

Solid-state NMR is potentially an ideal tool for the study of paramagnetism. However, until now, relatively few paramagnetic molecules or materials have been studied by high-resolution solid-state NMR methods based on magic-angle spinning (MAS) techniques.[1−17] Focusing on paramagnetic metal complexes, we should cite the studies on lanthanide acetates by Bryant et al.[1−3] and on copper dimers and trimers by Haw et al.[4,5] that started in the 1980s. More recently, Dobson et al. studied rare-earth pyrochlore stannates[6−8] as well as lanthanide acetates.[9,10]

The scarcity of such studies is due to the presence of unpaired electrons inducing rapid nuclear relaxation via electronic relaxation. This leads most often to spectra having large line widths and to the existence of numerous rotational sidebands arising from the (usually large) anisotropy of the hyperfine interactions. These effects therefore translate into practical difficulties with sensitivity and spectral resolution. This also changes very significantly the experimental conditions with respect to those used classically in diamagnetic samples.

In following Dobson et al.[9,10] for ^{13}C experiments, we have considered three different contributions to line width specific to paramagnetic molecules:

(i) Broadening of the ^{13}C lines due to the strong coupling of their spins with the electron spins.

(ii) Broadening due to the distribution of the internal fields associated with the difference in susceptibility between the powder and the surrounding gas (in our case, argon) in the rotor.[9−11,18,19] This contribution, discussed in some detail by Dobson et al.[9,10] and earlier in diamagnetic samples by Garroway[9,10,20,21] and Lippmaa,[22] is due to second-order effects associated with the so-called anisotropic bulk magnetic susceptibility (ABMS) of the samples.

(iii) Broadening due to incomplete proton decoupling in all samples containing organic molecules. In effect, solid-state proton NMR line widths are much larger in paramagnetic molecules than in diamagnetic ones due to dominant hyperfine interactions. Therefore, even with high-power decoupling, these interactions cannot usually be completely averaged out, leaving relatively broad ^{13}C lines.

Dobson et al.[10] demonstrated in the compounds they studied that the third contribution to the line widths is the strongest, the ABMS contribution the second most powerful, and the rapid electron relaxation the weakest. Therefore, to gain resolution in the study of paramagnetic molecules, they proposed the use of fully deuterated samples. The residual dipolar $^{13}C-^{2}D$ interactions are then quite efficiently averaged to zero by magic-angle rotation.

In this article, our purpose is to show the importance of similar high-resolution MAS ^{13}C solid-state NMR studies on a

* Corresponding author. Phone and Fax: (33) 04 76 88 41 36. E-mail: lamotte@drfmc.ceng.cea.fr.

† Service de Chimie Inorganique et Biologique.

‡ Present address: Laboratoire d'Analyses Chimiques et Radiométriques, Service d'Etude et de Modélisation des Procédés, Département de Recherche sur le Retraitement et la Vitrification, CEA de la Vallée du Rhône, BP 171, 30207 Bagnols-sur-Cèze Cedex, France.

§ Present adress: Rhodia, Etablissement Silicones Lyon, 55 rue des frères Perret, BP 22, 69191 St Fons cedex, France.

∥ Laboratoire des Lésions des Acides Nucléiques.

⊥ Laboratoire de Stéréochimie et des Interactions Moléculaires.

10.1021/jp002005o CCC: $19.00
Published on Web 10/13/2000

family of iron−sulfur complexes, the [4Fe−4S] cluster cubanes. These cubanes are of compelling interest in bioinorganic chemistry since they constitute model compounds for the active sites of ubiquitous metalloproteins.[23−25] In these electron transfer proteins, the basic cluster appears commonly in three different redox states $[4Fe-4S]^{n+}$ ($n = 1-3$). The exchange coupling between the high-spin iron atoms ($S = {}^5/_2$ for Fe(III) and 2 for Fe(II)) results in an $S = 0$ magnetic ground state for the oxidation-state $[4Fe-4S]^{2+}$, an $S = {}^1/_2$ ground state for $[4Fe-4S]^{3+}$, and $S = {}^1/_2$ or ${}^3/_2$ for $[4Fe-4S]^{1+}$, as established by EPR and Mössbauer spectroscopies at low temperatures (∼4 K).

Solution-state NMR (essentially of protons) has been extensively used to study these iron−sulfur proteins and, more specifically, the magnetic structure of their cubane active sites (see, for instance, refs 26−31 and references therein). The main source of information is measurements of temperature dependence, albeit over the limited temperature range (∼30 K) around room temperature, for the paramagnetic shifts of the β-CH_2 and α-CH protons of the cysteinyl residues binding the active site of the cluster to the protein amino acid backbone. These shifts result from the hyperfine interactions between the unpaired electron spins and the nuclei under observation. They therefore reflect the electron spin distribution on the cluster and ligand atoms resulting from the contributions of both ground and excited spin states, populated according to the Boltzmann law. In contrast, with ENDOR (the high-resolution method adjunct to EPR most often used to measure hyperfine interaction tensors) the iron−sulfur clusters are studied around liquid helium temperature to counter the very rapid increase of electronic relaxation times with temperature. As a consequence, only the hyperfine interactions relative to the ground magnetic state are probed.

Oxidized ferredoxins or reduced high-potential (HiPIP) proteins have their prosthetic site in the $[4Fe-4S]^{2+}$ state with ground spin state $S = 0$. Significant paramagnetic shifts of the β-CH_2 protons of the cysteins are still observed by NMR at room temperature due to hyperfine contributions from the populated first excited states.[27] Magnetic susceptibility measurements in synthetic model compounds indicate for this state that paramagnetism arises from ∼50−70 K.[32,33]

Applying solid-state NMR to these clusters is interesting because this method presents some specific advantages. First, it allows for the measurement of paramagnetic shifts over a large range of temperatures (150 K). This is essential to deriving accurately the spin coupling parameters and, thereby, the cluster magnetic spin ladder. Second, in solution, molecular motion (such as the conformational and fluxional dynamics of the ligands in the synthetic complexes or local dynamics in the protein in the vicinity of the prosthetic group) can lead to partial averaging of some shifts. In contrast, such movements only occur in solids in special cases. This allows direct comparison of the experimental results obtained in a well-defined and fixed geometry of the compound (known from the X-ray structure) with theoretical model calculations carried out for this geometry. Finally, solid-state NMR gives access not only to the isotropic shifts but also to the principal values of the shift tensor.

Rather than the proteins themselves, we chose to start our studies with synthetic model compounds due to the problems of sensitivity and resolution discussed above. To begin with, the present article is devoted to the study of the $[4Fe-4S]^{2+}$ state. This state has the simplest magnetic structure of the three and, therefore, the simplest ladder of magnetic levels. We present studies of two synthetic analogues of the [4Fe−4S] protein active sites and, in addition, a homologous [4Fe−4Se] complex. The first complex studied is $[(C_2Hs)_4N]_2[Fe_4S_4(SCH_2C_6H_5)_4]$ (**I**). Its relevance lies in the fact that it contains CH_2 groups at the level of the thiolate ligands which constitute good analogues of the β-CH_2 groups of cysteins in iron−sulfur proteins. For sensitivity reasons, it was necessary to specifically enrich the CH_2 groups of that compound with ^{13}C and, moreover, to prepare it in both fully deuterated (**I_D**) and fully protonated (**I_H**) forms. The second complex, $[(C_2H_5)_4N_{12}[Fe_4S_4(SC(CH_3)_3)_4]$ (**II**), presents a structure of high (D_{2d}) symmetry.[34] For this reason and also because it gives sharper lines than the previous one, studies were carried out at a natural abundance of ^{13}C. Note that this compound allows paramagnetic shift measurements of both the quaternary *t*-Bu carbon (simulating the β-CH_2 carbons of cysteins) and the terminal methyl *t*-Bu groups (simulating the α-CH carbons of cysteins). Finally, we also studied $[(C_2H_5)_4N]_2[Fe_4Se_4(SC(CH_3)_3)_4]$ (**III**), a homologue to the previous compound with its cubane ("inorganic") sulfur atoms substituted by selenium. Some of the relevant distances pertaining to compounds **I**−**III** are presented in Table 1.

TABLE 1: Interatomic Distances of $[(C_2H_5)_4N]_2[Fe_4S_4(SCH_2C_6H_5)_4]$ (I_H)[42] Idealized to $C2v$ Symmetry and of $[(C_2H_5)_4N]_2[Fe_4S_4(SC(CH_3)_3)_4]$ (II)[34] and $[(C_2H_5)_4N]_2[Fe_4Se_4(SC(CH_3)_3)_3]$ (III)[a]

	Fe−Fe	Fe−S* (or Fe−Se*)	Fe−S	S−C
I_H	∼2.776 Å (×2)	∼2.310 Å (×8)	∼2.251 Å (×4)	∼1.832 Å (×4)
	∼2.732 Å (×4)	∼2.239 Å (×4)		
II	2.764 Å (×2)	2.294 Å (×8)	2.254 Å (×4)	1.870 Å (×4)
	2.749 Å (×4)	2.274 Å (×4)		
III	2.817 Å (×2)	2.417 Å (×8)	2.248 Å (×4)	1.985 Å (×4)
	2.812 Å (×4)	2.274 Å (×4)		

[a] The expression "×*n*" indicates the multiplicity (i.e., *n*) of equal (or nearly equal) bond distances. An asterisk (*) denotes the inorganic sulfur or selenium atoms [Fe_4S_4*] or [Fe_4Se_4*].

II. Experimental Section

1. Preparation of $[(C_2H_5)_4N]_2[Fe_4S_4(S^{13}CH_2C_6H_5)_4]$ (I_H) and $[(C_2D_5)_4N]_2[Fe_4S_4(S^{13}CD_2C_6D_5)_4]$ (I_D). The $HS^{13}CH_2C_6H_5$ thiol was prepared from 98% enriched $^{13}CO_3Ba$ following a procedure involving five successive reactions.[35] The deuterated thiol $HS^{13}CD_2C_6D_5$ was prepared in the same way by using perdeuterated bromobenzene to form the labeled benzoic acid. $LiAlD_4$ was used instead of $LiAlH_4$ to reduce benzyl benzoate to benzyl alcohol. Then **I_H** and **I_D** were prepared following the classical synthesis procedure of Christou and Garner.[36] In the case of **I_D**, we used $(C_2D_5)_4NI$ to introduce the counterion, whose preparation is also described in ref 35. The purity and integrity of the isotope enrichment of the samples were verified by standard solution NMR at each of the different steps of the preparation of the ligands and of the complexes.

2. Preparation of $[(C_2H_5)_4N]_2[Fe_4S_4(SC(CH_3)_3)_4]$ and $[(C_2H_5)_4N]_2[Fe_4Se_4(SC(CH_3)_3)_4]$. Both compounds were prepared following the classical synthesis procedure of Christou and Garner.[36]

3. Solid-State NMR Methodology. The experiments were carried out on a Bruker MSL 200 spectrometer. In a glovebox under an argon atmosphere (1 ppm of O_2), the polycrystalline powder samples were packed in 7 mm zirconia rotors and tightly closed with boron nitride caps. Variable-temperature experiments were carried out between 180 and 330 K using the VT-1000 unit and the MAS-DB pneumatic unit. ^{13}C NMR shifts are given with respect to TMS, whose peak position has been obtained with a static rotor filled with a mixture of TMS and acetonitrile. The temperature recorded at the level of the

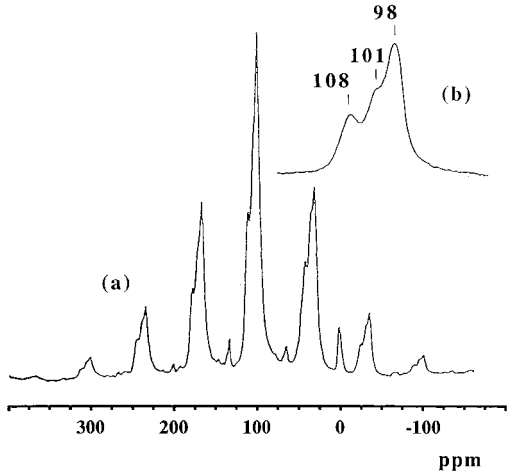

Figure 1. 50 MHz ^{13}C-MAS NMR spectrum of $[(C_2D_5)_4N]_2[Fe_4S_4(S^{13}CD_2C_6D_5)_4]$ (**I$_D$**) at room temperature. (a) Complete spectrum with its rotational sidebands. In addition to the broad main peaks due to the enriched ^{13}C of the thiolate CD_2 groups, small and sharp peaks appear. They are due to the natural abundance of ^{13}C atoms pertaining to the phenyl groups or to the counterions. (b) Enlarged view of the central, "isotropic" group. Three peaks can be distinguished at 108, 101, and 98 ppm, the latter line having an intensity roughly double that of the two others.

thermocouple of the MAS probe was calibrated (as a function of rotor speed) and corrected by using the temperature dependence of the isotropic chemical shift measured from ^{207}Pb-MAS spectra of $Pb(NO_3)_2$.[37] This lead compound was placed in a separate rotor and used as an external reference as it is not chemically compatible with our [4Fe−4S] complexes.

Several pulse sequences were used, depending on the sample studied and whether the isotropic shifts of the different ^{13}C's or the principal components of their anisotropic tensors were to be primarily measured. For **I$_H$**, we have tested the applicability of the classical CP-MAS sequence. Since the T_1 relaxation times of the ^{13}C in these paramagnetic samples (especially those of the β-carbon adjacent to the sulfur thiolate atoms) are in the millisecond range while those of the corresponding ^{1}H might be even shorter, the cross-polarization (CP) process between ^{1}H and ^{13}C may be very inefficient. By measuring the ^{13}C signal as a function of the contact CP time τ using the CP-MAS sequence, we have found this signal to be maximum for $\tau \approx 100$ μs with a rapid decrease after $\tau \approx 500$ μs. Under these conditions, no net gain in sensitivity can be obtained by cross polarization from the protons to the ^{13}C; rather, there is a loss in sensitivity. Therefore, the 1D spectra used for the measurement of the ^{13}C isotropic shifts of **I$_H$** were obtained under magic-angle rotation (MAS) between 2.5 and 4 kHz using a $\pi/2$ ^{13}C pulse followed by detection under strong ($\omega_1 \approx 80$ kHz) proton decoupling. The corresponding 1D spectra of **I$_D$** were obtained by a simple $\pi/2$ ^{13}C pulse and MAS, this last procedure being sufficient to average out the ^{13}C−^{2}D dipolar interactions. To measure the components of the anisotropic shift tensors, we used a 2D magic-angle turning (MAT) sequence yielding correlation of isotropic−anisotropic shifts.[38,39] In this case, low-speed rotations (between 0.5 and 1.5 kHz) were used, resulting in spectra composed of a large collection of rotational sidebands, thus optimizing the determination of the anisotropic components.[40]

III. Results for the $[(C_2D_5)_4N]_2[Fe_4S_4(S^{13}CD_2C_6D_5)_4]$ Complex

1. Isotropic ^{13}C Shifts. Figure 1 presents the ^{13}C-MAS spectrum obtained from a powder of $[(C_2D_5)_4N]_2[Fe_4S_4(S^{13}CD_2C_6D_5)_4]$ (**I$_D$**) at room temperature. It is composed of a central "isotropic" group of poorly resolved lines (identified by the fact that its position is independent of the rotor speed, see Figure 1), flanked by several rotational sidebands of similar shape. A closer examination of this central group of lines (see Figure 1b) shows that it corresponds to the superposition of two lines centered at $\delta_{iso} = 108$ and 101 ppm with a third line of double intensity centered at 98 ppm. Individual line widths are ∼250 Hz. Despite this broadening, the spectrum is easily obtained owing to ^{13}C enrichment and to the fact that we can pulse and accumulate rapidly because the T_1 values are short (3.2, 3.6, and 4.1 ms for the three peaks, respectively). These lines correspond to the ^{13}C of the CD_2 groups of the four thiolate ligands surrounding the [4Fe−4S] cluster, two of them corresponding to the line at 98 ppm. Relatively similar spectra can be obtained from **I$_H$** but with such a loss of resolution that the three peaks mentioned above cannot be distinguished. This confirms the importance of using fully deuterated samples for MAS studies of paramagnetic molecules.[10,41]

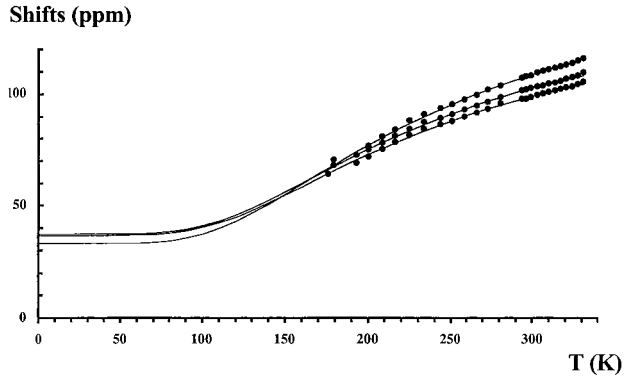

Figure 2. Temperature dependence and best fits of the position of the isotropic ^{13}C resonance peaks of the CD_2 groups for $[(C_2D_5)_4N]_2[Fe_4S_4(S^{13}CD_2C_6D_5)_4]$ (**I$_D$**). To relate these CH_2 carbon atoms directly to those belonging to the cysteinyl ligands of the [4Fe−4S] clusters, we followed the same conventional labeling used for proteins by calling them "β" (see also the caption of Table A in Supporting Information).

MAS spectra similar to those of Figure 1 have been recorded for **I$_D$** sample as a function of temperature. As in Figure 1, three peaks with relative intensities 1:1:2 are again observed over the whole temperature range. The temperature dependence of their positions δ_{iso} is reported in Figure 2 (the corresponding data are reported as Supporting Information in Table A). As expected, we observe that the shift values decrease when the temperature decreases, i.e., when the populations of the paramagnetic excited states of the ladder of magnetic states decrease. Moreover, two carbon atoms remain equivalent throughout the temperature range, while the two others differ somewhat. However, the differences in the values of the shifts of the four carbon atoms are small and can be related to the crystallographic structure of that compound published by Averill et al.[42]

In effect, this [4Fe−4S] cubane has nearly, but not exactly, D_{2d} symmetry and exhibits a compressed structure along an axis perpendicular to two cubane faces. This last axis corresponds to a near, but not exact, S_4 symmetry, as can be seen from the interatomic distances reported in Table 1. To a good degree of approximation, the Fe_1, $C_1(H_2)$, and S_5 atoms on one hand and the Fe_2, $C_2(H_2)$, and S_6 atoms on the other hand are located in one common plane. The same holds true for the Fe_3, $C_3(H_2)$, and S_7 atoms and the Fe_4, $C_4(H_2)$, and S_8 atoms, located in a second plane perpendicular to the first one, both planes intersecting around the S_4 axis. Actually, complete loss of

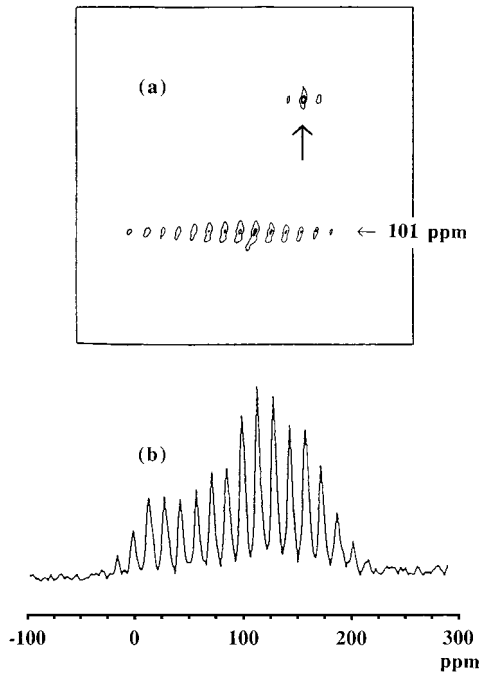

Figure 3. 2D ^{13}C magic-angle turning correlation spectrum at room temperature between isotropic and anisotropic shifts for $[(C_2H_5)_4N]_2[Fe_4S_4(S^{13}CH_2C_6H_5)_4]$ ($\mathbf{I_H}$). (a) 2D map with isotropic shifts along the vertical axis and sideband powder spectra along the horizontal axis. The resonance peaks marked by a vertical arrow in that 2D map are due to the strongest sharp line at ~0 ppm observed in Figure 1. They probably correspond to the natural abundance of ^{13}C atoms in the terminal methyl groups of counterions. (b) 1D slow-spinning sideband powder spectrum corresponding to the slice at 101 ppm of the 2D map.

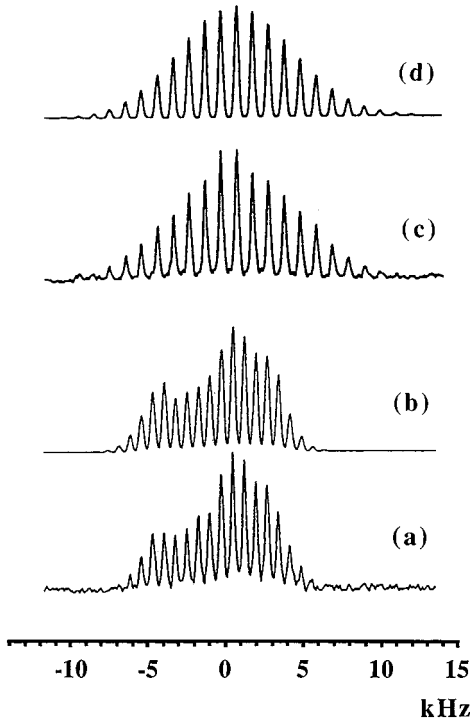

Figure 4. Comparison between the anisotropic projection of the 2D ^{13}C correlation spectrum of the protonated $[(C_2H_5)_4N]_2[Fe_4S_4(S^{13}CH_2C_6H_5)_4]$ ($\mathbf{I_H}$) with that obtained for the deuterated $[(C_2D_5)_4N]_2[Fe_4S_4(S^{13}CD_2C_6D_5)_4]$ ($\mathbf{I_D}$): (a) spectrum for $\mathbf{I_H}$, (b) simulation for $\mathbf{I_H}$, (c) spectrum for $\mathbf{I_D}$, and (d) simulation for $\mathbf{I_D}$.

symmetry (due to crystal packing effects) only appears clearly at the level of the relative orientations of the terminal groups of the benzyl thiolate, i.e., of their phenyl rings. This can be expressed in terms of the Fe−S−C(H_2)−C(phenyl ring) dihedral angles of each thiolate ligand. Referring to the atomic positions given in the crystallographic study,[42] their values are 200°, 250°, 240°, and 264° for the $Fe_1-S_5-C_1-C_{phenyl}$, the $Fe_2-S_6-C_2-C_{phenyl}$, the $Fe_3-S_7-C_3-C_{phenyl}$, and the $Fe_4-S_8-C_4-C_{phenyl}$ dihedral angles, respectively. Therefore, while the geometry of the ligand conformations with respect to the Fe−S cluster is equivalent within 10° at the levels of C_2, C_3, and C_4, it is quite different at the level of C_1. Since a symmetric $[4Fe-4S]^{2+}$ state of D_{2d} symmetry can be represented as two $Fe^{2.5+}-Fe^{2.5+}$ mixed-valence pairs perpendicular to the S_4 axis,[43] we are led to formulate the hypothesis that the two equivalent ^{13}C atoms resonating at 98 ppm at room temperature are the C_3 and C_4 atoms belonging to the thiolate ligated to Fe_3 and Fe_4, respectively. This leaves the inequivalent C_1 and C_2 atoms corresponding to the two peaks at 108 and 101 ppm (at this same temperature), respectively, without specifying which corresponds to which.

2. Anisotropies of the ^{13}C Shifts. 2D ^{13}C correlation spectra between isotropic and anisotropic shifts were obtained with the MAT sequence[38,39] for $\mathbf{I_H}$ (cf. Figure 3). From slices extracted along the anisotropic axis, we deduced the three components of the anisotropic shift tensors for the ^{13}C of the thiolate CH_2 groups, each tensor being the sum of a diamagnetic chemical shift tensor σ_{dia} and a paramagnetic shift tensor σ_{para}. Comparison of such a trace (Figure 3b, reproduced in Figure 4a) with the analogous trace obtained for $\mathbf{I_D}$ (Figure 4c) shows that the deuterated sample exhibits an envelope of all the sidebands with no distinctive feature of the shift anisotropy. This is attributed to the inhomogeneous broadening caused by the C−D dipolar coupling. While it is therefore advantageous for the isotropic shift resolution to record MAS spectra in deuterated paramagnetic molecules rather than in the protonated ones, the reverse is true when measuring their anisotropic components (unless the deuterium can be decoupled, which is neither easy nor routinely available).

Since we obtain useful 2D correlation spectra only for $\mathbf{I_H}$, which displays moreover unresolved isotropic peaks for the four different carbons, we obtained only average, and thus approximate, principal components (σ_1, σ_2, σ_3) for their anisotropic shifts. As their isotropic shifts are not far from equivalent, we can suppose that the same holds true for their anisotropic parts. The relative order of magnitude of the principal components is defined by $|\sigma_3 - \sigma_{iso}| \geq |\sigma_2 - \sigma_{iso}| \geq |\sigma_1 - \sigma_{iso}|$. We calculate the anisotropy parameter $\alpha = \sigma_3 - \sigma_{iso}$ as well as the asymmetry parameter $\eta = (\sigma_2 - \sigma_1)/\sigma_{iso}$ by iterative fitting of the experimental spectra to simulations calculated with the analytical expressions of Herzfeld and Berger.[44,45] In Figure 4b we show such a simulation corresponding to the best fit to the experimental spectrum of Figure 4a. Taking the values of α and η and adding a Gaussian broadening to the sideband envelope to crudely factor the $^{13}C-^{2}D$ dipolar interactions in the CD_2 groups, we obtained a similar simulation (shown in Figure 4d) for $\mathbf{I_D}$, which may be compared with the experimental spectrum of Figure 4c. In Figure 5, we report the temperature dependence of the three principal values of the four (total) ^{13}C shift tensors, treated as equivalent, obtained from fits to a series of MAT experiments performed on the protonated compound.

IV. Results for the $[(C_2H_5)_4N]_2[Fe_4S_4(SC(CH_3)_3)_4]$ and $[(C_2H_5)_4N]_2[Fe_4Se_4(SC(CH_3)_3)_4]$ Complexes

The $[(C_2Hs)_4N]_2[Fe_4S_4(SC(CH_3)_3)_4]$ compound (**II**), as said before, is especially interesting because its cluster is of high

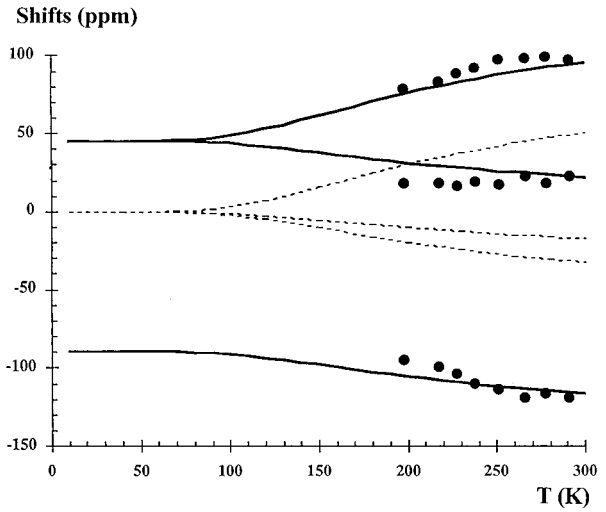

Figure 5. Experimental points and estimated temperature dependencies (continuous lines) of the three principal values of the four ^{13}C total shift tensors considered as equivalent for $[(C_2Hs)_4N]_2[Fe_4S_4(S^{13}CH_2C_6Hs)4]$ ($\mathbf{I_H}$). The continuous lines correspond to the three total components (diamagnetic chemical shift plus paramagnetic shift), while the dotted lines correspond only to their crudely calculated paramagnetic shift contributions.

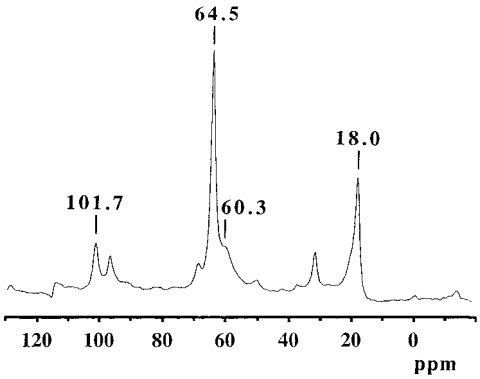

Figure 6. 50 MHz ^{13}C-MAS NMR spectrum of the natural abundance of $[(C_2H_5)_4N]_2[Fe_4S_4(SC(CH_3)_3)_4]$ (**II**) at room temperature. All the unlabeled peaks correspond to rotational sidebands.

symmetry.[34] The crystal symmetry is tetragonal $I\bar{4}2m$, and the cubane center is coincident with the center of symmetry of the unit cell. The Fe−S distances are very similar to those of **I**, as seen in Table 1. The cubane is compressed along the *c* (and also S_4) axis, and it has exact D_{2d} symmetry. This symmetry also relates all the other atoms of the ligands and counterions of the structure. Therefore, the spectrum under MAS and proton decoupling of that compound, presented in Figure 6, is very simple. Moreover, it is, in that case, easily obtained without ^{13}C enrichment because it involves a small number of inequivalent carbon atoms and also because its lines are sharper (∼60 Hz) than those of **I**.

Peaks are observed at 101.7, 64.5, and 18 ppm; a fourth, broader peak appears at 60.3 ppm, at the foot of the intense peak at 64.5 ppm. Their integrated intensities are in the ratio of 1:3:2:2. The line at 101.7 ppm is thus attributed to the 4 quaternary carbon atoms of the *t*-Bu thiolate ligands labeled C(1),[34] and the line at 64.5 ppm is attributed to the 12 methyl carbon atoms of these same ligands, thus respecting the 1:3 ratio. In the published crystallographic structure,[34] 2 possible positions (labeled C(2) and C(3)) are actually given for these 3 methyl carbons. This is because, at the level of each ligand, the 8 (out

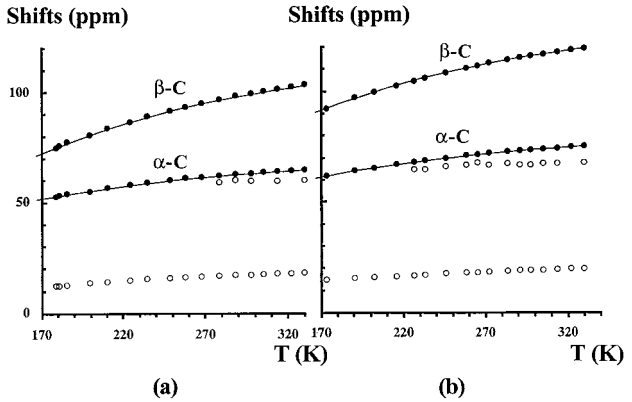

Figure 7. Temperature dependencies and best fits of the positions of the different isotropic ^{13}C resonance peaks for (a) $[(C_2H_5)_4N]_2[Fe_4S_4(SC(CH_3)_3)_4]$ (**II**) and (b) $[(C_2H_5)_4N]_2[Fe_4Se_4(SC(CH_3)_3)_4]$ (**III**). To relate the quaternary and methyl carbon atoms directly to those belonging to the cysteinyl ligands of the [4Fe−4S] clusters, we chose to follow the same conventional labeling used for proteins by calling them "β" and "α", respectively. Closed circles correspond to the resonance peaks of the β-C and α-C of the *t*-Bu ligands, while open circles correspond to those of the methylene and methyl carbons of the counterions.

of 12) carbons named C(2) pertain to 2 different carbons corresponding to each other by the plane of symmetry between the (equivalent) *x* and *y* axes of the crystal, while the 4 remaining carbons (C(3)) are contained in this symmetry plane. The two lines at 60.3 and 18.0 ppm are attributed to the eight methylene atoms (labeled C(4)) and eight methyl carbon atoms (labeled C(5a) and C(5b)) of the $(C_2H_5)_4N^+$ counterions, respectively. In the structure, the C(5a) and C(5b) positions refer to disordered positions of their terminal methyl groups.[34]

Concerning $[(C_2H_5)_4N]_2[Fe_4Se_4(SC(CH_3)_3)_4]$ (**III**), we found its crystal symmetry to be also tetragonal $I\bar{4}2m$, isomorphic with **II**. The most relevant distances are given in Table 1. On the basis of Fe−Fe distances, this cubane can be described as nearly regular and only very faintly compressed along the *c* axis, while it appears more compressed when Fe−Se distances are considered. The ^{13}C spectrum under MAS and proton decoupling appears to be very similar to that of **II**, leading to identical assignments of the different peaks.

Panels a and b of Figure 7 show the temperature dependence of the different lines for **II** and **III**, respectively (the corresponding data are reported in Tables B1 and B2 in Supporting Information). Several remarks can be made about these results. First, it is interesting to notice that both types of carbons located next to the thiolate sulfur have similar shift values, i.e., the C(1) carbons in **II**, and the $C(H_2)$ atoms in compound I. Their temperature dependencies are also similar.

A second remark is that in **II** and **III**, we never observe (over the temperature range studied) two separate peaks of respective intensities 8 and 4 for C(2) and C(3) but only a single narrow resonance of intensity 12. This clearly indicates that the carbon atoms of the terminal methyl groups of the *t*-Bu thiolate ligands are all equivalent and, therefore, that the *t*-Bu's of the thiolate ligands are rotating rapidly at the present NMR time scale. Additionally, the singleness and sharpness of the line of the terminal methyl groups of the tetraethylammonium counterions indicate that some movement (probably correlated to those of the *t*-Bu groups) also exists at their level, rendering them completely equivalent. Therefore, these experiments clearly indicate that molecular movements exist in these two compounds in the solid state. This fact may also explain the occurrence of high-crystalline and molecular symmetries[46] for **II** and **III**. This

may also be related to the fact that the density of **II** is lower (1.19)[34] than those of other typical [4Fe−4S] synthetic analogues (∼1.40). The temperature variations of the peak associated with the (rotating) (C(2)) + (C(3)) carbons therefore constitute a valuable model of the behavior expected for the ^{13}C resonance of the corresponding α-CH cystein carbons in proteins. Finally, we should mention that in the spectrum of Figure 6 (and also in the spectrum of **III**, not shown), we observe many fewer sidebands than in Figure 1 for **I**. This is certainly related to the fact that the shift anisotropies are very appreciably averaged by the movements in the crystal discussed above. This is why we have not tried to measure and study the anisotropies for **II** and **III**.

V. Interpretation and Discussion

In a paramagnetic molecule or complex, the chemical shift of a given nucleus *i* is given (in parts per million) by

$$\delta_{tot}(i) = \delta_{dia}(i) + \delta_{para}(i) \tag{1}$$

where $\delta_{dia}(i)$ is the diamagnetic chemical shift and $\delta_{para}(i)$ the paramagnetic shift due to the hyperfine interaction between its nuclear spin and the spin distribution of unpaired electrons. When clusters constituted by an assembly of monometallic complexes are considered, it has been established, first in dimers[47,48] and thereafter in polymetallic complexes,[27] that the hyperfine interactions (measured, for instance, by EPR or Mössbauer spectroscopy) and the ensuing NMR paramagnetic shifts result from magnetic coupling among the monomer spins are directly related via the spin coupling coefficient *K* to the (intrinsic) hyperfine interactions in these monomers. Moreover, since these magnetic couplings generate ladders of magnetic energy levels characterized by their spin states, the paramagnetic shifts result from the contributions to the hyperfine interactions of all these levels, populated according to the Boltzmann law. We briefly address these elements in two following paragraphs, considering the special case of the $[4Fe-4S]^{2+}$ cluster.

1. Theoretical Background: Spin Coupling Structure and Spin States of the $[4Fe-4S]^{2+}$ Cluster. The $[4Fe-4S]^{2+}$ cubane formally contains two high-spin ferric and two high-spin ferrous ions of $S = {}^5/_2$ and 2, respectively.[49] Mössbauer spectroscopy performed on this state indicates, however, that the four iron ions are generally equivalent, thus carrying a common charge of 2.5+ (refs 50 and 51). This is understood as a consequence of full delocalization of each of the two six d electrons of the ferrous ions over mixed-valence pairs (noted as "12" and "34"). Spin coupling of the different monomer electron spins occurs through the interplay of exchange terms.[49] These are mainly of two sorts: the super-exchange *J* terms, which result in iron−sulfur clusters in antiferromagnetic coupling between the metal (or monomer) spins, and the double-exchange *B* terms favoring resonance delocalization (and thus ferromagnetism) within mixed-valence pairs (see eq 2 below). One describes therefore the spin coupling within the cubane in two steps, first by coupling the iron spins of the two pairs (Fe_1-Fe_2 and Fe_3-Fe_4) with ${}^1/_2 \le S_{12},S_{34} \le {}^9/_2$. Both pairs of spins are then coupled again to yield the total spin *S* of the cluster, with $0 \le |S_{12} - S_{34}| \le S \le S_{12} + S_{34} \le 9$, yielding the spin state $|S_{12},S_{34},S\rangle$. The pairwise delocalization process is accounted for in the spin Hamiltonian[52] by double-exchange terms, B_{12} and B_{34}, in conjunction with the operators V_{12} and V_{34} reproducing the correct spin dependence of this energetic gain and with the transfer operators T_{12} and T_{34} transferring the electron from one site to the other within a mixed-valence pair (see ref 52 for further mathematical details).

The magnetic spin levels, of corresponding spin states $|S,Ms\rangle$, are characterized by their energies $E(S_{12},S_{34},S) = \langle S_{12},S_{34},S|H|S_{12},S_{34},S\rangle$, computed after spin coupling, i.e., relying on the following appropriate spin Hamiltonian *H*:

$$H = \sum_{i<j} J_{i,j} \vec{S}_i \vec{S}_j - B_{12}V_{12}T_{12} - B_{34}V_{34}T_{34} \tag{2}$$

where the constant $J_{i,j}$ stands for the (super-) exchange coupling between spins $\vec{S}_i$ and $\vec{S}_j$. Additionally, synthetic model compounds of the $[4Fe-4S]^{2+}$ state are known usually to display a compression of the cubane along a direction perpendicular to two iron pairs (chosen as Fe_1-Fe_2 and Fe_3-Fe_4), rationalized on theoretical grounds[43] (see Table 1). As can be seen in Table 1, this is the case for **I**, **II**, and **III**. This distortion implies that the geometrical arrangement of the iron ions departs from an ideal tetrahedron (where all Fe−Fe distances are equal). Since the four iron ions bear the same formal charge, 2.5+, this geometrical compression can be accounted for (as first-order) by assuming[53] that $J_{i,j} = J$ for $i,j = (13,14,23,24)$ whereas $J_{12} = J + \Delta J_{12}$ and $J_{34} = J + \Delta J_{34}$. This model provides us with analytical solutions to the Heisenberg part of the spin Hamiltonian. In effect, the energy levels $E(S_{12},S_{34},S)$ associated with this spin Hamiltonian are then given by

$$E(S_{12},S_{34},S) = \frac{J}{2}S(S+1) + \frac{\Delta J_{12}}{2}S_{12}(S_{12}+1) + \frac{\Delta J_{34}}{2}S_{34}(S_{34}+1) \pm B_{12}\left(S_{12}+\frac{1}{2}\right) \pm B_{34}\left(S_{34}+\frac{1}{2}\right) \tag{3}$$

It must be noted that at this level of approximation, we do not distinguish among $Fe^{2+}-Fe^{2+}$, $Fe^{2+}-Fe^{3+}$, and $Fe^{3+}-Fe^{3+}$ pairs and the corresponding *J* values. We can finally set $\Delta J_{12} = \Delta J_{34} \equiv \Delta J$ and $B_{12} = B_{34} \equiv B$ in eq 4 for symmetry reasons.

2. Expression of the Paramagnetic Shift for Ligand Nuclei of Polymetallic Clusters. Let us consider again a ^{13}C nucleus *i* belonging to monomer *k* (with metallic ion spin S_k) embedded in the polymetallic [4Fe−4S] cluster. The expression of the paramagnetic chemical shift $\delta_{para}(i)$ is then given by

$$\delta_{para}(i) = \frac{g_e\beta_e a^k_{iso}(i)}{g_n\beta_n 3kT} \frac{\sum_S K^k_S S(S+1)(2S+1)\exp(-E(S)/kT)}{\sum_S (2S+1)\exp(-E(S)/kT)} \tag{4}$$

where a^k_{iso} is the intrinsic hyperfine coupling constant of the ^{13}C nucleus in the absence of spin coupling and K^k_S is a spin projection coefficient quantifying the projection of the local spin S_k (of the monomer *k* bearing the ^{13}C nucleus *i*) onto the total spin *S* of the system in the spin state $|S_{12},S_{34},S\rangle$. See refs 48 and 54 for similar expressions derived in the context of solution NMR. Numerically, the term in front of the temperature-dependent ratio is $41877a^k_{iso}(i)/T$, with $a^k_{iso}(i)$ in MHz, *T* in K, and $\delta_{para}(i)$ in ppm. At this stage, each experimental curve can be fitted by this model containing two adjustable parameters $\delta_{dia}(i)$ and $a^k_{iso}(i)$ in addition to the energetic *J*'s and *B*'s entering explicitly into the expression of $E(S)$.

3. Fits of the Temperature Variations of the Isotropic Shifts. The *J*, Δ*J*, and *B* terms are the energetically relevant parameters for a fitting procedure. An important issue in modeling the electronic and magnetic structure of this cluster

TABLE 2: Parameter Values Obtained for $[(C_2H_5)_4N]_2[Fe_4S_4(SCH_2C_6H_5)_4]$ (I), $[(C_2H_5)_4N]_2[Fe_4S_4(SC(CH_3)_3)_4]$ (II), and $[(C_2H_5)_4N]_2[Fe_4Se_4(SC(CH_3)_3)_4]$ (III) for the Different Types of Fits Defined in the Text[a]

	fit 1a	fit 1b	fit 2a	fit 2b	fit 3a	fit 3b
			compound **I**			
J (cm^{-1})	596	509	433	413	428	412
B (cm^{-1})	–	–	652	579	–	–
ΔJ (cm^{-1})	–	–	–	–	−139	−125
δ_{dia} (ppm)	49.1	32	33.0	32	32.3	32
δ_{dia} (ppm)	51.1	32	37.2	32	36.6	32
δ_{dia} (ppm)	49.9	32	36.7	32	36.2	32
a_{iso} (MHz)	2.74	2.61	3.51	3.20	3.44	3.15
a_{iso} (MHz)	2.37	2.42	3.03	2.97	2.98	2.92
a_{iso} (MHz)	2.25	2.29	2.88	2.81	2.83	2.77
erf	1.492	2.597	1.322	1.556	1.320	1.551
			compound **II**			
J (cm^{-1})	573	476	383	373	382	369
B (cm^{-1})	–	–	425	468	–	–
ΔJ (cm^{-1})	–	–	–	–	84	−93
δ_{dia} (ppm)	62.1	49	48.9	49	49.4	49
δ_{dia} (ppm)	47.2	36	41.5	36	41.7	36
a_{iso} (MHz)	1.59	1.53	1.74	1.70	1.66	1.62
a_{iso} (MHz)	0.69	0.86.	0.75	0.95	0.72	0.91
erf	0.323	1.439	0.258	1.094	0.257	1.094
			compound **III**			
J (cm^{-1})	568	410	373	295	365	290
B (cm^{-1})	–	–	535	499	–	–
ΔJ (cm^{-1})	–	–	–	–	112	−103
δ_{dia} (ppm)	81.8	49	67.4	49	66.3	49
δ_{dia} (ppm)	56.3	36	49.1	36	48.5	36
a_{iso} (MHz)	1.41	1.63	1.69	1.64	1.64	1.58
a_{iso} (MHz)	0.7.1	0.93	0.85	0.93	0.83	0.90
erf	0.386	1.488	0.281	0.536	0.280	0.527

[a] Fits "a" and "b" refer to unconstrained (resp. constrained) δ_{dia} values. erf denotes the standard (i.e., in the mean-square sense) error function.

is the relative order of magnitude of these three different terms. This has been thoroughly discussed in recent years[55−59] and has remained somewhat controversial.

One approach[43,60,61] considers that the double-exchange B terms are the leading factors responsible for the electronic structures adopted by [4Fe−4S] clusters ($B \leq 1000$ cm^{-1} for iron−sulfur clusters). Extrapolating to this limit, we have $B \gg |\Delta J|$ (the "limit" since ΔJ, necessarily non-zero when distortions occur, would still intervene as a perturbation). We could therefore analyze our experimental data by imposing $|\Delta J| \approx 0$ to the first order while keeping J and B as the only adjustable parameters.

At the opposite limit, a second approach considers the pair exchange terms of the J and ΔJ as the most important, the double-exchange mechanism being only present to delocalize the electrons within the pairs (thus, $0 \leq B \ll |\Delta J|$ with B a few 10 cm^{-1} at most).[58] We could therefore also fit the data at the limit where $B \approx 0$ while keeping J and ΔJ adjustable.

The two approaches are not visibly mutually exclusive, and the best method probably lies somewhere between the two limits (by necessity, $B \neq 0$ since there is delocalization and, when distortions occur, $\Delta J \neq 0$). This is why we proceeded to the fit of our experimental curves using three models, referred to as "fit 1" ($B = 0$, $\Delta J = 0$, J-only model), "fit 2" ($B \neq 0$, $\Delta J = 0$), and "fit 3" ($B = 0$, $\Delta J \neq 0$).

The results of the three kinds of fits are presented in Table 2 for **I**−**III**.[62] In fit 1, J is found between 410 and 509 cm^{-1} when the $\delta_{dia}(i)$ constants are constrained to their solid-state experimental value of 32 ppm[63] (see the column "fit 1b" in Table 2). This J value is in reasonably good agreement with that derived from the fits of magnetic susceptibility curves measured for $(Et_4N)_2[Fe_4S_4(SPh)_4]$: 464 cm^{-1}, again with a J-only model.[33] When left free, the values for the $\delta_{dia}(i)$ parameter generally tend to be higher than those expected and measured in either the liquid or solid phases (compare columns "fit 1a" and "fit 1b" in Table 2). Moreover, the J values are higher than those obtained by constraining $\delta_{dia}(i)$. For constrained data, we finally notice the regular drop of J from **I** (509 cm^{-1}) to **III** (410 cm^{-1}).

When B or ΔJ (fit 2 or 3) is introduced, J drops to 290−413 cm^{-1}, almost irrespective of the fit used (2 or 3) for constrained $\delta_{dia}(i)$, and to 365−433 cm^{-1} for unconstrained $\delta_{dia}(i)$. Again, a progression toward smaller values is observed upon going from **I** to **III**. The diamagnetic shift values are now in much better agreement with directly measured ones (except for **III**). B is found to be significant between 425 and 652 cm^{-1}. The same is true for the corresponding ΔJ values in model 3, found between −84 and −139 cm^{-1}. To check the reliability of the exchange parameter values determined from our fitting procedure and also to test the sensitivity of the fits to the values of the diamagnetic constants, we made the latter parameters vary around their optimal values (48.9 and 41.5 ppm) for **II** (see Table C in Supporting Information) in fit 2. As can be seen, a variation of ±10% for one or both δ_{dia} around the optimal value leaves almost unchanged the J values ($\delta J/J \approx \pm 4\%$), whereas B is much more sensitive ($\delta B/B \leq \pm 21\%$).

Finally, the intrinsic hyperfine coupling constants $a^k_{iso}(i)$ are found between 2.8 and 3.2 MHz for β-carbons in **I**, again irrespective of the fit (2 or 3). Those hyperfine constants turn out to be smaller in the case of both **II** and **III**—that is, ∼1.7 MHz for the quaternary carbon and ∼0.8 MHz for the methyl carbons.

As seen above, we have found that fitting procedure 2 yields positive B values whereas fit 3 yields negative ΔJ values. In both cases, this means that the ground state is made up of two mixed-valence iron pairs with maximum spins S_{12} and S_{34}, i.e., the spins are ferromagnetically ordered within each pair, the resulting spins of the two pairs being antiferromagnetically coupled. The situation is very similar in the first excited states which involve the large spins S_{12} and S_{34}. The ground state is thus $|^9/_2,^9/_2,0\rangle$, and the first excited state, separated from the ground state by J, turns out to be $|^9/_2,^9/_2,1\rangle$. The first excited states whose energies are determined by either B or ΔJ are the degenerate states $|^9/_2,^7/_2,1\rangle$ and $|^7/_2,^9/_2,1\rangle$ at B above the first excited state $|^9/_2,^9/_2,1\rangle$ for model 2 and at $-4.5\Delta J$ above $|^9/_2,^9/_2,1\rangle$ for model 3. We have represented in Figure 8 the spin-state ladders obtained for **I** from the Hamiltonian involving J and B (model 2) and J and ΔJ (model 3). A striking feature is that both models yield the same spin-state ladder up to ∼2000 cm^{-1}! Effectively, both models appear in practice to be equivalent and experimentally indistinguishable since within the range of temperatures considered, the levels above this limit are virtually unpopulated and do not contribute significantly to the paramagnetic shifts. Below ∼2000 cm^{-1}, the identity of the two spin ladders can be rationalized by setting $B \equiv -^9/_2\Delta J$. Further justification and discussion of this "covariance effect" between the two exchange parameters B and ΔJ in the $[4Fe-4S]^{2+}$ cluster is reported in the Appendix. Note also from Figure 8 that the J values are much more precisely determined than B or ΔJ, the population of the first excited state contributing to the paramagnetic shift being much greater than those originating from the two next (degenerate) excited states.

It is therefore important to notice that in the case of this $[4Fe-4S]^{2+}$ cluster, these NMR experiments alone do not allow us to discriminate between models 2 and 3 because of the exact

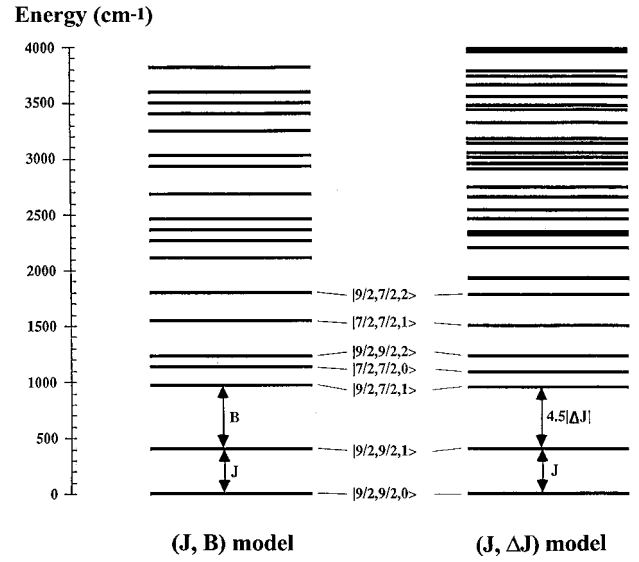

Figure 8. Magnetic spin ladders derived for $\mathbf{I_D}$ using the (J,B) model (left) and the (J,ΔJ) model (right). Note that only the lowest spin states have been listed.

equivalence of the spin-state ladders when $B = -{}^9/_2\Delta J$. This also means that any combination of B_o and ΔJ_o satisfying the constraint that $B_o - {}^9/_2\Delta J_o$ is constant (this constant being B if deduced from fit 2 or $-4.5\Delta J$ if deduced from fit 3) will result in the same energy level diagram up to ∼2000 cm^{-1}. This covariance between B and ΔJ for the magnetic energy levels is special to this $[4Fe-4S]^{2+}$ state. It does not exist in the cases of the 1+ or 3+ redox states of the [4Fe−4S] cluster, for which the respective effects of B and ΔJ can be clearly discriminated.

This motivated us to investigate this matter using the density functional theory (DFT) and the broken symmetry (BS) technique to estimate the $J/\Delta J$ exchange coupling constants and compare them to B (results unpublished). We briefly summarize here our findings thus obtained. A ratio $\Delta J/J$ of ∼17% is predicted for **I**, against ∼10% for **II** in agreement with the greater or lesser compression observed in the cluster geometries. B values are always computed at ∼600 cm^{-1}. This yields the $4.5|\Delta J|/(B + 4.5|\Delta J|)$ ratios of 0.31 for **III** and 0.43 for **II** (being aware of the fact that DFT-computed J values are usually overestimated by a factor 2).

4. Anisotropic Parts of the Chemical Shift Tensors of Compound I. Let us now consider the anisotropic part of the shift tensors and their temperature variation estimated for **I**, reported in Figure 5. A serious problem is the separation of the diamagnetic tensor from the paramagnetic (hyperfine) tensor because their principal axes must be different. The main (and useful) difference between both tensors is that the principal components of the paramagnetic tensor must vary with temperature, while it is reasonable to suppose that those of the diamagnetic tensor do not vary much (since we have no indication of appreciable movement of the ligands in **I**). The anisotropic hyperfine tensor results essentially from dipolar contributions arising from the (thermalized) spin density distribution over the [4Fe−4S] cluster. In single-crystal proton ENDOR studies, we have previously analyzed experimental anisotropic hyperfine tensors using a multipole point−dipole approximation to deduce the ground-state spin density distribution in the oxidized[35] $[4Fe-4S]^{3+}$ and reduced[64] $[4Fe-4S]^{+}$ centers. In this solid-state NMR study of $[4Fe-4S]^{2+}$ centers, we will consider first the diamagnetic shift tensor as unknown and proceed to compute the anisotropic hyperfine tensors from the temperature-dependent spin density distribution.

A [4Fe−4S] cluster can be viewed as an assembly of four "FeS_4" monomers sharing some of their sulfur atoms. For a given spin state, the integrated spin density of a monomer k is simply given by the corresponding spin projection coefficient K_S^k. It has been established elsewhere[65] that this integrated spin density is then distributed over the atoms composing each monomer through spin delocalization—that is, ∼70% remaining on the iron, whereas ∼30% is (roughly speaking) shared equally with the four coordinating sulfurs. A thiolate sulfur exhibits therefore a spin density of roughly $0.3K_S^k/4$, whereas that of an inorganic S* sulfur is the sum of three contributions from the three adjacent iron sites. Moreover, taking the four K_S^k's as equal ($^1/_4$; cf. section V-5) in all the levels of the ladder is a reasonable approximation, since isotropic ^{13}C shifts are found to be only slightly inequivalent. Thus, relying on the atomic positions from the crystallographic structure[42] and on the ladder of energy levels of Figure 8, we could calculate the anisotropic ^{13}C hyperfine interactions from the spin populations on the iron and sulfur atoms.[66]

The results of these calculations of the temperature dependence of the three principal components of paramagnetic tensors (dotted lines) are presented in Figure 5. Close to zero at low temperature (the $S = 0$ ground state being diamagnetic), these components keep increasing in magnitude in much the same way as the isotropic shifts. To match these curves with the experimental points, we have to add some temperature-independent diamagnetic contribution to each component to get the full tensor. We have chosen such values to obtain the best fit of the total estimated tensor (continuous lines in Figure 5) to the experimental points. This crude approach gives a roughly axial diamagnetic shift tensor with the three estimated principal components of +90, −45, and −45 ppm and yields a rather satisfying quality of fit. We could not obtain more precise information, especially on its principal directions, as the experimental data are not sufficient for such a task. This explains the slight disagreement between the experimental points and the continuous lines because, very probably, both hyperfine and diamagnetic tensors do not possess the same principal axes.

5. Connection with Magnetic Susceptibility Measurements. There is a peculiar feature which can be exploited to simplify the expression of the solid-state NMR shift in the special case of the $[4Fe-4S]^{2+}$ cluster of (or close to) D_{2d} symmetry. In effect, for all the spin states $|S_{12},S_{34},S\rangle$ for which $S_{12} = S_{34}$, the four carbon atoms correspond to the same spin projection coefficients $K_S^k = {}^1/_4$ and $k = 1-4$ since

$$\begin{cases} K_S^1 = K_S^2 = \dfrac{1}{2}\left[\dfrac{S(S+1) + S_{12}(S_{12}+1) - S_{34}(S_{34}+1)}{2S(S+1)}\right] \\ K_S^3 = K_S^4 = \dfrac{1}{2}\left[\dfrac{S(S+1) + S_{34}(S_{34}+1) - S_{12}(S_{12}+1)}{2S(S+1)}\right] \end{cases} \quad (5)$$

Moreover, for those states with $S_{12} \neq S_{34}$, there is a systematic energetic degeneracy between two states with permuted pair spin values (of the type $|S_a,S_b,S\rangle$ and $|S_b,S_a,S\rangle$, $S_a \neq S_b$). This is due to the symmetry of the spin Hamiltonian itself (that is, $\Delta J_{12} = \Delta J_{34}$ and $B_{12} = B_{34}$). For a given ^{13}C nucleus belonging to k, one finds in the numerator of the corresponding paramagnetic shift the two contributing terms (both multiplied by the common factor of $S(S + 1)(2S + 1)\exp(-E(S)/kT)$)

$$K^k_{S_A} + K^k_{S_B} = {}^1/_2 \tag{6}$$

There is therefore a formal contribution of $^1/_4$ for each of the two degenerate states, as if $S_{12} = S_{34}$. All K^k_S's in eq 2 can therefore be set formally to $^1/_4$. Factorizing them out allows us to write for each individual ^{13}C nucleus i (with $\Sigma K^k_S = 1$) as

$$\delta_{\text{para}}(i) = \frac{g_e\beta_e a^k_{\text{iso}}(i)}{g_n\beta_n 12kT} \frac{\sum_S S(S+1)(2S+1)\exp(-E(S)/kT)}{\sum_S (2S+1)\exp(-E(S)/kT)} \tag{7}$$

At this stage, we must point out that the expression of the (molar) paramagnetic susceptibility is very similar:

$$\chi_{\text{para}} = \frac{(g_e\beta_e)^2}{3kT} \frac{\sum_S S(S+1)(2S+1)\exp(-E(S)/kT)}{\sum_S (2S+1)\exp(-E(S)/kT)} \tag{8}$$

The prefactor of eq 8 is $0.5/T$ in cgs units. There is therefore a close analogy between the temperature dependence of magnetic susceptibility and that of solid-state NMR shifts. The main difference between them lies in the absence or presence of the spin projection coefficient K^k_S. This difference emphasizes the fact that the solid-state NMR technique uses local probes (^{13}C nuclei), whereas the susceptibility is a measure of the global magnetization of the sample. This is the reason, apart from differences in the experimental temperature ranges, that we can in principle derive ("global") magnetization data from ("local") solid-state NMR data, whereas the reverse is not possible without knowledge of local parameters such as the intrinsic hyperfine coupling constants or diamagnetic constants. In this way, it becomes clear why the (paramagnetic) NMR traces seemed to be proportional to the susceptibility. Therefore, in the very special case of a $[4Fe-4S]^{2+}$ cluster, each individual NMR trace associated to each carbon nucleus is proportional to the susceptibility. Of course, as will be shown elsewhere, this result does not hold for $[4Fe-4S]^{1+/3+}$ clusters where the information available is much richer than that from susceptibility measurements.

It is now appropriate to fit anew the susceptibility data published in the literature for **I**[32] with a model including both exchange and double-exchange terms because in no case is a fit based on a single J value satisfactory over the entire temperature interval of measurement.[32] We use for that the 12 experimental points given in Table XIII of ref 32 within the temperature range of 50−338 K.

We used the following fit function:

$$\chi = \chi_{\text{TIP}} + w_i \frac{(g_e\beta_e)^2 S_i(S_i+1)}{3kT} + (1-w_i)\chi_{\text{para}} \tag{9}$$

where χ_{TIP} stands for the temperature-independent paramagnetic term, w_i measures the weight of a $S_i = {}^5/_2$ impurity, and χ_{para} is given in eq 8. As the published data have been already corrected for impurity, we expect throughout $w_i \approx 0$ (as indeed found in our fits). We thus obtained $\chi_{\text{TIP}} \approx 52 \times 10^{-5}$ cgsu and $J \approx 496$ cm^{-1} for fit 1 (J-only), whereas for fits 2 and 3, we found $\chi_{\text{TIP}} \approx 42 \times 10^{-5}$ cgsu, $J \approx 347$ cm^{-1}, $B = 645$ cm^{-1}, and $\Delta J \approx -145$ cm^{-1} (notice again that $B \approx -4.5\Delta J$). We had from solid-state NMR for **I** that $J \approx 430$ cm^{-1}, $B \approx 652$ cm^{-1}, and $\Delta J \approx -139$ cm^{-1}, in very good agreement. Despite recovering compatible fit parameter values from both susceptibility and solid-state NMR, the latter technique is more reliable than the former in our view. In effect, there is no need for impurity correction, whereas susceptibility samples without any impurity are not easily prepared. Moreover, as already emphasized, fitting NMR data yields knowledge not only of the magnetic energy levels but also of the detailed structure of the spin states (through K^k_S): If this distinction is not that spectacular for the $[4Fe-4S]^{2+}$ redox state, it is indeed so for the corresponding reduced cluster. Finally, ^{13}C solid-state NMR shifts and subsequent fits yield additional information in the form of local terms such as a_{iso} and δ_{dia}, which can be checked independently by other techniques.

VI. Conclusions

We have demonstrated that ^{13}C solid-state NMR constitutes a good method of determining the magnetic spin ladder of [4Fe−4S] clusters and, therefore, an interesting tool for the reliable estimation of the corresponding energetic parameters (J, B, and ΔJ) which describe their magnetic properties. We are confident that the present results are transposable to the proteins in the $[4Fe-4S]^{2+}$ redox state; the parameters and the ladder of magnetic levels determined here constitute the basis for the interpretation of their magnetic properties. The published (solution) NMR study of the ferredoxin of *Clostridium acidi urici* with two [4Fe−4S] cubane active sites[67] allows for such a comparison. The authors found there paramagnetic shifts of 75 ± 15 ppm for the β-carbons (β-C) of cysteines at 293 K (data corrected for the diamagnetic contribution). With its CH_2 groups, **I** mimics the cysteine $\beta-CH_2$, and as it turns out, the paramagnetic shifts that we measured by solid-state NMR are, on average, $\delta_{\text{para}}(\beta\text{-C})_{\text{av}} \approx \delta_{\text{tot}}(\beta\text{-C})_{\text{av}} - 32 \approx 77 \pm 6$ ppm at 295 K (cf. Table 1), in excellent agreement with the protein data. The dispersion on these shift values for the different cystein ligands is 2.5 times larger than for the thiolate groups of **I**. This reflects the less symmetric environment of the cubanes in the protein than in the model compound.

Moreover, it appears clearly from our experimental results and from their subsequent theoretical analysis that B is as large as J. However, since it is only essentially determined by the upper temperature range of the δ_{para} temperature dependence (i.e., the upper part of the magnetic spin ladder) and because of the covariance between B and ΔJ, it must be pointed out that its determination is only approximate for this $[4Fe-4S]^{2+}$ case. The importance of B has been further tested in similar solid-state NMR studies of the $[4Fe-4S]^{1+}$ ($S = {}^1/_2$ and $^3/_2$) redox state, which we recently concluded. It will be shown that no covariance ambiguity exists for these two $[4Fe-4S]^{1+}$ spin states. Moreover, the fitting parameter B appears for both spin states in the energetics (cf. section V-1) as well as in wave function coefficients. This double constraint offers a firm ground for the determination of the value of B (within the approximations set for the analysis of the solid-state NMR data).

VII. Appendix

To understand exactly the covariance between B and ΔJ in $[4Fe-4S]^{2+}$ clusters, we consider the energy difference between a generic spin state $|S_{12},S_{34},S\rangle$ and the ground state $|^9/_2,^9/_2,0\rangle$

$$E(S_{12},S_{34},S) - E(^9/_2,^9/_2,0) = \frac{J}{2}S(S+1)\begin{cases}+B\Delta S_{12} & +B\Delta S_{34} \\ +\dfrac{\Delta J}{2}\Delta S_{12}(\Delta S_{12}-10) & +\dfrac{\Delta J}{2}\Delta S_{34}(\Delta S_{34}-10)\end{cases} \quad \text{(A1)}$$

where $\Delta S_{i,j} = {}^9/_2 - S_{i,j}$ (i,j = 12,34). Notice that model 2 presents a linear variation of the energies in the spin pairs $S_{i,j}$ (i.e., $B\Delta S_{i,j}$), whereas model 3 exhibits a quadratic variation (i.e., $(\Delta J/2)\Delta S_{i,j}(\Delta S_{i,j} - 10)$). One thus expects a non-zero value of $\Delta S_{i,j}$ (the case $\Delta S_{i,j} = 0$ being trivial) for which the two contributions are equal (this is analogous to saying that a straight line and a parabolic curve can cross at no more than two points). Therefore, when B is equated with $(\Delta J/2)(\Delta S_{i,j} - 10)$, it becomes clear that within the subset of states $|S_{12},S_{34},S\rangle$ defined by $\Delta S_{i,j} = 1$ (i.e., S_{12} and/or $S_{34} = {}^7/_2$), the two model-dependent energetic contributions become exactly equal under the numerical condition

$$\frac{B}{\Delta J} = \frac{\Delta S_{i,j} - 10}{2} = -\frac{9}{2} \quad \text{(A2)}$$

More generally, given a state $|S_{12}°,S_{34}°,S°\rangle$ (with $S_{12}° = S_{34}°$), all the states $|S_{12},S_{34},S\rangle$ such that $\Delta S_{12} = S_{12}° - S_{12} = \{0,1\}$ and $\Delta S_{34} = S_{34}° - S_{34} = \{0,1\}$ define a subset of all the spin ladder states whithin which the application of the relation $B = -S_{12}°\Delta J$ results in identical energy level diagrams.

In the case of a $[4Fe-4S]^{2+}$, the first state for which both models 2 and 3 do not result in identical energy levels must have S_{12} (and/or equivalently S_{34}) equal to at least ${}^5/_2$ ($\Delta S_{i,j} > 2$). Among the lowest spin states with $S_{12} = {}^5/_2$, we therefore consider $|{}^5/_2,{}^9/_2,2\rangle$ (of relative energy $(3J + 2B)/(3J - 8\Delta J)$ with respect to the ground state), $|{}^5/_2,{}^7/_2,1\rangle$ ($(J + 3B)/(J - 12.5\Delta J)$), and $|{}^5/_2,{}^5/_2,0\rangle$ ($4B/(-16\Delta J)$) because they satisfy two conditions: S_{34} is large (since $B > 0$ and $\Delta J < 0$) and S is small ($J > 0$). Their corresponding energies are all calculated to be >1900 cm^{-1} for **I**. Therefore, from an experimental point of view, it is exactly equivalent to fit the data considering all the possible spin states or restricting the fit to those of the subset defined above (i.e., with $\Delta S_{i,j} = \{0,1\}$).

This remarkable feature is obviously coincidental, since it depends on the (quite large) values of the parameters J and $B/\Delta J$ in the magnetic system. This can be illustrated by considering the oxidized $[4Fe-4S]^{3+}$ cluster. An appropriate energy expression is as follows:[68]

$$E(S_{12},S_{34},S) = \frac{J}{2}S(S+1)\begin{Bmatrix}-B_{12}(S_{12}+{}^1/_2) \\ \dfrac{\Delta J_{12}}{2}S_{12}(S_{12}+1)\end{Bmatrix} + \frac{\Delta J_{34}}{2}S_{34}(S_{34}+1) \quad \text{(A3)}$$

If $|{}^9/_2,4,{}^1/_2\rangle$ is the ground state, an equivalence of the spin-state energies will be expected within the subset for which $\Delta S_{12} = 0,1$ ("12" referring to the mixed-valence pair)—that is, $B_{12} = -({}^9/_4)\Delta J_{12}$. But this covariance affects only part (that concerning the mixed-valence pair), not all (as for the 2+ cluster), of the spin-state energy. Magnetic susceptibility fits revealed that the spin state $|{}^5/_2,2,{}^1/_2\rangle$ ($\Delta S_{12} = 2$) lies well below the limit of 2000 cm^{-1} (see Scheme 1 of ref 69). As a consequence, the fact that the two energy level diagrams, derived from the two fits (one involving B_{12} and one involving ΔJ_{12}), look similar is simply due to the fact that the physical system for which we try to reconstruct the spin-state ladder is obviously the same in both fitting procedures. One may not therefore speak soundly of a "covariance" relation in such cases,[70] except to indicate correlated trends between parameters, in contrast to the exceptional $[4Fe-4S]^{2+}$ case detailed above for which such a behavior is exactly followed experimentally by all the thermally accessible states.

Acknowledgment. The authors thank Mrs. Marya Desfonds for the preparation of the seleniated compound **III** and Dr. Jacques Pécaut for the crystallographic parameters of this compound.

Supporting Information Available: Numerical values of the chemical shifts as functions of temperature for the ^{13}C resonance peaks and a test of the reliability of the exchange parameters of fit 2. This material is available free of charge via the Internet at http://pubs.acs.org.

References and Notes

(1) Chacko, V. P.; Ganapathy, S.; Bryant, R. G. *J. Am. Chem. Soc.* **1983**, *105* (5), 5491−5492.
(2) Ganapathy, S.; Chacko, V. P.; Bryant, R. G.; Etter, M. C. *J. Am. Chem. Soc.* **1986**, *108*, 3159−3165.
(3) Ganapathy, S.; Bryant, R. G. *J. Magn. Reson.* **1986**, *70*, 149−152.
(4) Campbell, G. C.; Haw, J. F. *Inorg. Chem.* **1988**, *27*, 3706−3709.
(5) Campbell, G. C.; Reibenspies, J. H.; Haw, J. F. *Inorg. Chem.* **1991**, *30*, 171−176.
(6) Cheetham, A. K.; Dobson, C. M.; Grey, C. P.; Jakeman, R. J. B. *Nature* **1987**, *328*, 706−707.
(7) Grey, C. P.; Dobson, C. M.; Cheetham, A. K.; Jakeman, R. J. B. *J. Am. Chem. Soc.* **1989**, *111*, 505−511.
(8) Grey, C. P.; Smith, M. E.; Cheetham, A. K.; Dobson, C. M.; Dupree, R. *J. Am. Chem. Soc.* **1990**, *112*, 4670−4675.
(9) Clayton, A. N.; Dobson, C. M.; Grey, C. P. *J. Chem. Soc., Chem. Commun.* **1990**, 72−74.
(10) Brough, A. R.; Grey, C. P.; Dobson, C. M. *J. Am. Chem. Soc.* **1993**, *115*(5), 7318−7327.
(11) Stoll, M. E.; Majors, T. J. *Phys. Rev.* **1981**, *B24*, 2859−2862.
(12) Nayeem, A.; Yesinowski, J. P. *J. Chem. Phys.* **1988**, *89*, 4600−4608.
(13) Liu, K.; Ryan, D.; Nakanishi, K.; McDermott, A. *J. Am. Chem. Soc.* **1995**, *117*, 6897−6906.
(14) Spaniol, T. P.; Kubo, A.; Terao, T. *J. Chem. Phys.* **1997**, *106*, 5393−5405.
(15) Hentsch, F.; Helmle, M.; Köngeter, D.; Mehring, M. *Phys. Rev.* **1988**, *B37*, 7205−7208.
(16) Michel, P.; Moradpour, A.; Penven, P.; Firlej, L.; Bernier, P.; Levy, B.; Ravy, S.; Zahab, A. *J. Am. Chem. Soc.* **1990**, *112*, 8285−8292.
(17) Mustarelli, P.; Massarotti, V.; Bini, M.; Capsoni, D. *Phys. Rev.* **1997**, *B55*, 12018−12024.
(18) Schwerk, U.; Michel, D.; Pruski, M. *J. Magn. Reson.* **1996**, *A119*, 157−164.
(19) Kubo, A.; Spaniol, T. P.; Terao, T. *J. Magn. Reson.* **1998**, *133*, 330−340.
(20) Garroway, A. N.; VanderHart, D. L.; Earl, W. L. *Philos. Trans. R. Soc. London* **1981**, *A299*, 609−628.
(21) VanderHart, D. L.; Earl, W. L.; Garroway, A. N. *J. Magn. Reson.* **1981**, *44*, 361−401.
(22) Alla, M.; Lippmaa, E. *Chem. Phys. Lett.* **1982**, *87*, 30−33.
(23) Johnson, M. K. In *Encyclopedia of Inorganic Chemistry*; King, R. B., Ed.; Wiley: New York, 1994; Vol. 4, pp 1896−1915.
(24) Beinert, H.; Holm, R. H.; Münck, E. *Science* **1997**, *277*, 653−659.
(25) Lamotte, B.; Mouesca, J.-M. *C. R. Acad. Sci. Paris* **1997**, *324*, 117−132.
(26) Bertini, I.; Ciurli, S.; Luchinat, C. *Struct. Bonding* **1995**, *83*, 1−54.
(27) Bertini, I.; Luchinat, C. *NMR of Paramagnetic Substances*; Elsevier: Amsterdam, 1996; Vol. 150.
(28) Wang, P. L.; Donaire, A.; Zhou, Z. H.; Adams, M. W. W.; LaMar, G. N. *Biochemistry* **1996**, *35*, 11319−11328.
(29) Calzolai, L.; Gorst, C. M.; Bren, K. L.; Zhou, Z. H.; Adams, M. W. W.; LaMar, G. N. *J. Am. Chem. Soc.* **1997**, *119*, 9341−9350.
(30) Huber, J. G.; Moulis, J.-M.; Gaillard, J. *Biochemistry* **1996**, *35*, 12705−12711.

(31) Kyritsis, P.; Huber, J. G.; Quinkal, I.; Gaillard, J.; Moulis; J.-M. *Biochemistry* **1997**, *36*, 7839−7846.

(32) Laskowski, E. J.; Frankel, R. B.; Gillum, W. O.; Papaefthymiou, G. C.; Renaud, J.; Ibers, J. A.; Holm, R. H. *J. Am. Chem. Soc.* **1978**, *100*, 5322−5337.

(33) Papaefthymiou, G. C.; Laskowski, E. J.; Frota-Pessôa, S.; Frankel, R. B.; Holm, R. H. *Inorg. Chem.* **1982**, *21*, 1723−1728.

(34) Mascharak, P. K.; Hagen, K. S.; Spence, J. T.; Holm, R. H. *Inorg. Chim. Acta* **1983**, *80*, 157−170.

(35) Mouesca, J.-M.; Rius, G.; Lamotte, B. *J. Am. Chem. Soc.* **1993**, *115* (5), 4714−4731.

(36) Christou, G.; Garner, C. D. *J. Chem. Soc., Dalton Trans.* **1979**, 1093.

(37) Bielecki, A.; Burum, D. P. *J. Magn. Reson.* **1995**, *A116*, 215−220.

(38) Gann, S. L.; Baltisberger, J. H.; Pines, A. *Chem. Phys. Lett.* **1993**, *210*, 405−410.

(39) Hu, J. Z.; Alderman, D. W.; Ye, C.; Pugmire, R. J.; Grant, D. M. *J. Magn. Reson.* **1993**, *A105*, 82.

(40) Hodgkinson, P.; Emsley, L. *J. Chem. Phys.* **1997**, *107*, 4808.

(41) Clayton, A. N.; Dobson, C. M.; Grey, C. P. *J. Chem. Soc., Chem. Commum.* **1990**, 72−74.

(42) Averill, B. A.; Herskovitz, T.; Holm, R. H.; Ibers, J. A. *J. Am. Chem. Soc.* **1973**, *95*, 3523−3534.

(43) Bominaar, E. L.; Hu, Z.; Münck, E.; Girerd, J.-J.; Borshch, S. A. *J. Am. Chem. Soc.* **1995**, *117*, 6976−6989.

(44) Herzfeld, J.; Berger, A. E. *J. Chem. Phys.* **1980**, *73*, 6021.

(45) Hodgkinson, P.; Emsley, L. *Prog. NMR Spectrosc.* **2000**, *36*, 201.

(46) In **II** and **III**, we have tried to determine with X-rays toward the low temperatures whether these rotations of the *t*-Bu groups and the movements of the methyl carbons of the counterions become blocked. In effect, at 90 K, the two compounds present a new phase and a different structure of lower symmetry than that observed at 300 K. This structure is fairly complicated (probably triclinic but with α, β, and γ angles very close to 90°), and it probably contains a large number of inequivalent molecules. We have been unable to solve it without ambiguity. The change from this low-symmetry phase to the phase described at room temperature occurs at ∼120−130 K for **II** and ∼150−160 K for **III**. Therefore, these X-ray observations confirm that the movements in the solid state and especially the rotations of the *t*-Bu groups of the thiolate ligands are operative in the whole range of temperatures where we perform these solid-state NMR experiments.

(47) Bencini, A.; Gatteschi, D. *EPR of Exchange Coupled Systems*; Springer-Verlag: Berlin, 1990.

(48) Banci, L.; Bertini, I.; Luchinat, C. *Structure and Bonding*; Springer-Verlag: Berlin, 1990; Vol. 72, pp 113−136.

(49) Noodleman, L.; Peng, C. Y.; Case, D. A.; Mouesca, J.-M. *Coord. Chem. Rev.* **1995**, *144*, 199−244.

(50) Middleton, P.; Dickson, D. P. E.; Johnson, C. E.; Rush, J. D. *Eur. J. Biochem.* **1978**, *88*, 135.

(51) Middleton, P.; Dickson, D. P. E.; Johnson, C. E.; Rush, J. D. *Eur. J. Biochem.* **1980**, *104*, 289−296.

(52) Papaefthymiou, V.; Girerd, J.-J.; Moura, I.; Moura, J. J. G.; Münck, E. *J. Am. Chem. Soc.* **1987**, *109*, 4703.

(53) It is important in effect to recognize that for the problem treated here, ΔJ terms arise because of geometrical distortions and not because of differences in formal iron charges. In other words, ΔJ varies continuously upon increasing the compression of the structure from zero (as it should be if all Fe−Fe distances were equal) to any value $J_{Fe^{2.5+}-Fe^{2.5+}} = J + \Delta J$, whereas one would expect well-defined (and possibly transferable) ranges of values for $J_{Fe^{2+}-Fe^{2+}}$, $J_{Fe^{2+}-Fe^{3+}}$, and $J_{Fe^{3+}-Fe^{3+}}$ exchange couplings in other $[4Fe-4S]^{1+/3+}$ systems.

(54) Bertini, I.; Turano, P.; Vila, A. J. *Chem. Rev.* **1993**, *93*, 2833−2932.

(55) Blondin, G.; Girerd, J.-J. *JBIC* **1996**, *1*, 170−172.

(56) Kröckel, M.; Grodzicki, M.; Papaefthymiou, V.; Trautwein, A. X.; Kostikas, A. *JBIC* **1996**, *1*, 173−176.

(57) Noodleman, L.; Case, D. A.; Mouesca, J.-M.; Lamotte, B. *JBIC* **1996**, *1*, 177−182.

(58) Bertini, I.; Luchinat, C. *JBIC* **1996**, *1*, 183−185.

(59) Belinsky, M. I. *JBIC* **1996**, *1*, 186−188.

(60) Borshch, S. A.; Bominaar, E. L.; Blondin, G.; Girerd, J.-J. *J. Am. Chem. Soc.* **1993**, *115*, 5155−5168.

(61) Bominaar, E. L.; Borshch, S. A.; Girerd, J.-J. *J. Am. Chem. Soc.* **1994**, *116*, 5362−5372.

(62) Note that we only treat here the temperature variations of the β- and α-carbon atoms of compounds **II** and **III**. Comments relative to those of the counterion ^{13}C lines will be published in a separate note.

(63) The random coil ^{13}C chemical shift measured for the β-carbon of reduced cysteine is between 27 and 28 ppm, depending on the nearest-neighbor amino acid (Wishart et al. *J. Biomol. NMR*, **1995,** *5*, 67−81), whereas we measured it to be 32 ppm in the solid state. In the case of the *t*-Bu thiolate sodium salt, we measured 49 and 36 ppm for the quaternary and methyl carbon nuclei, respectively.

(64) Le Pape, L.; Lamotte, B.; Mouesca, J.-M.; Rius, G. *J. Am. Chem. Soc.* **1997**, *119*, 9771−9781.

(65) Mouesca, J.-M.; Noodleman, L.; Case, D. A.; Lamotte, B. *Inorg. Chem.* **1995**, *34*, 4347−4359.

(66) To estimate ^{13}C anisotropic hyperfine tensors wherein the CH_2 carbon p orbital pointing toward the thiolate sulfur bears some spin density leading to a non-negligible anisotropy contribution, we took this term explicitly into account, evaluating its relative weight from density functional calculations, in a manner described elsewhere. This is in contrast to the proton case, whose s orbitals do not allow for some local source of dipolar anisotropy. Results to be published.

(67) Bertini, I.; Capozzi, F.; Luchinat, C.; Piccioli, M.; Vila, A. J. *J. Am. Chem. Soc.* **1994**, *116*, 651−660.

(68) Noodleman, L. *Inorg. Chem.* **1988**, *27*, 3677−3679.

(69) Jordanov, J.; Roth, E. K. H.; Fries, P. H.; Noodleman, L. *Inorg. Chem.* **1990**, *29*, 4288−4292.

(70) Banci, L.; Bertini, I.; Briganti, F. Luchinat, C.; Scozzafava, A.; Vincens Oliver, M. *Inorg. Chem.* **1991**, *30*, 4517−4524.